IEEE Journal of Microwaves

Received 27 August 2020; revised 11 October 2020; accepted 21 October 2020.
Date of current version 7 January 2021.

Digital Object Identifier 10.1109/JMW.2020.3034578

Microwave Huygens' Metasurfaces: Fundamentals and Applications

VASILEIOS G. ATALOGLOU, MICHAEL CHEN, MINSEOK KIM, AND GEORGE V. ELEFTHERIADES (Fellow, IEEE)

(Invited Paper)

The Edward S. Rogers Department of Electrical and Computer Engineering, University of Toronto, Toronto, ON M5S 3G4, Canada

CORRESPONDING AUTHOR: George V. Eleftheriades (e-mail: gelefth@waves.utoronto.ca).

This work was supported by the Natural Sciences and Engineering Research Council (NSERC) of Canada.

ABSTRACT In this article, we review the topic of Huygens' metasurfaces with an emphasis on existing and emerging applications at microwave frequencies. Huygens' metasurfaces have demonstrated unprecedented capabilities of controlling electromagnetic wavefronts by means of electric and magnetic dipole moments arranged in a thin sheet. We present the fundamental principles of Huygens' metasurfaces based on the boundary conditions governing their operation. Then, we discuss the aspect of practical realization of Huygens' metasurfaces and the different types of constituent subwavelength scatterers (unit cells). Moreover, we summarize recent developments in several areas related to metasurfaces, such as perfect anomalous refraction, polarization control, antenna beamforming and reconfigurable metasurfaces. Lastly, we provide a brief outlook on emerging metasurface-based microwave technologies that are expected to further grow in the future.

INDEX TERMS Huygens' metasurfaces, equivalence principle, perfect refraction, thin lenses, polarization control, antenna beamforming, reconfigurable metasurfaces.

I. INTRODUCTION

In the past few years, research in the field of 'artificial' electromagnetic materials or 'metamaterials' has seen an explosive growth. The basic premise is to create structures that would induce an engineered distribution of electric and magnetic dipole moments upon illumination by an impinging electromagnetic field. Under certain conditions such as the constituent unit cells being sub-wavelength in size, these structures can be homogenized and described by desired macroscopic quantities such as a permittivity, a permeability and a refractive index. A comprehensive analytical treatment describing the early (sixties and earlier) related work on 'artificial dielectrics' can be found in the classical text by Robert E. Collin [1]. In the now about 20-year old field of metamaterials, the sought-after macroscopic quantities describe exotic properties such as a negative permittivity, a negative permeability, and a negative or a near-zero refractive index. The most representative metamaterial is the one characterized by a negative index of refraction, first demonstrated experimentally at microwave frequencies [2]–[4]. In the engineering community a transmission-line approach was developed for synthesizing metamaterials with distinct advantages such as reduced insertion losses and broader overall bandwidths [5], [6].

This review article describes some recent advances in the field of metasurfaces which can be thought to be two-dimensional (2D) metamaterials. It is interesting to note that the bulk of the work on metasurfaces has been chronologically conducted following the more general work on volumetric metamaterials. Arguably this area originated from the seminal work by Capasso and co-workers in the optical regime associated with the introduction of the 'generalized law of refraction' [7]. In particular, this current paper focuses on Huygens' metasurfaces (HMSs) which comprise 2D arrays of Huygens' sources or scatterers. Typically, these HMSs are embodied by co-located orthogonal electric and magnetic dipole moments. Such 2D metasurfaces should be homogenized with suitable quantities such as susceptibility or impedance/admittance tensors, as will be described below in more detail. Since wave propagation and associated phenomena such as refraction can be explained in terms of the Huygens' principle dating back to

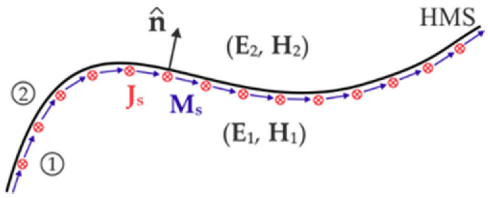

FIGURE 1. Schematic of a passive Huygens' metasurface. The induced current densities $\mathbf{J}_s$ and $\mathbf{M}_s$ support a discontinuity between the fields $\{\mathbf{E}_1, \mathbf{H}_1\}$ and $\{\mathbf{E}_2, \mathbf{H}_2\}$ at the two sides of the HMS.

the 17th century [8], HMSs are a natural way to engineer and control the shape of electromagnetic wavefronts, as will be described in this review article. Hence the appealing attributes of the HMSs are that they can achieve several of the full 3D metamaterial functionalities while being much simpler to physically realize and of lower profile.

In summary, this review article describes the fundamental theory and some of the applications of HMSs at microwave frequencies. As a disclaimer this review is by no means exhaustive and inevitably there is some bias toward emphasizing the work conducted in the research group of the authors.

II. BASIC THEORY OF HUYGENS' METASURFACES

Due to their electrically thin nature, Huygens' metasurfaces are macroscopically modeled through appropriate boundary conditions at an infinitesimally thin sheet, as depicted in Fig. 1. The basic HMS itself supports an electric and an orthogonal magnetic surface current density, denoted by $\mathbf{J}_s$ and $\mathbf{M}_s$, respectively [9]–[11]. In active HMSs, these surface current densities are implemented with impressed sources, while in the case of passive HMSs that are primarily covered in this review paper, they are passively excited by the incident tangential electric and magnetic fields. For two sets of stipulated fields $\{\mathbf{E}_1, \mathbf{H}_1\}$ and $\{\mathbf{E}_2, \mathbf{H}_2\}$ at the two sides of the HMS, the required electric and magnetic surface current densities are given as

$$\mathbf{J}_s = \hat{\mathbf{n}} \times (\mathbf{H}_2 - \mathbf{H}_1)\,, \tag{1a}$$

$$\mathbf{M}_s = -\hat{\mathbf{n}} \times (\mathbf{E}_2 - \mathbf{E}_1)\,, \tag{1b}$$

where the fields are calculated at the boundary of the discontinuity and $\hat{\mathbf{n}}$ is the normal unit vector towards region 2, as shown in Fig. 1.

In order to synthesize a HMS that supports a desired wave transformation, the discontinuity expressions in (1a)-(1b) should be supplemented with another set of expressions that relate the surface current densities to the total fields at the two sides of the HMS. This is achieved by a set of homogenized HMS parameters that take the form of surface polarizabilities, surface susceptibilities or surface impedances/admittances [12]–[14]. Although all representations are equivalent, the latter formulation is chosen in this paper and four independently defined second-order tensors are introduced; these are the surface electric impedance $\overline{\overline{Z}}_{\rm se}$, the surface magnetic admittance $\overline{\overline{Y}}_{\rm sm}$, the magnetoelectric coupling coefficient $\overline{\overline{K}}_{\rm em}$ and the electromagnetic coupling coefficient $\overline{\overline{K}}_{\rm me}$. The boundary conditions encapsulating the HMS response take the following form

$$\frac{1}{2}\left(\mathbf{E}_{t,1} + \mathbf{E}_{t,2}\right) = \overline{\overline{Z}}_{\rm se} \cdot \mathbf{J}_s - \overline{\overline{K}}_{\rm em} \cdot (\hat{\mathbf{n}} \times \mathbf{M}_s)\,, \tag{2a}$$

$$\frac{1}{2}\left(\mathbf{H}_{t,1} + \mathbf{H}_{t,2}\right) = \overline{\overline{Y}}_{\rm sm} \cdot \mathbf{M}_s + \overline{\overline{K}}_{\rm me} \cdot (\hat{\mathbf{n}} \times \mathbf{J}_s)\,, \tag{2b}$$

where the subscript t denotes the tangential to the HMS components of the fields and the dot products represent the matrix multiplications between a second order tensor and a 2×1 vector. It should be noted that normal induced electric or magnetic currents are not included in (2). Moreover, only the boundary conditions of the tangential components of the electric and magnetic fields are presented, as these are sufficient to describe the total fields at the two regions of the HMS, according to the uniqueness theorem. Lastly, in this review paper only reciprocal metasurfaces will be discussed. Imposing the requirement of reciprocity to the formulation presented in (2) and assuming for simplicity a planar metasurface normal to the z axis, the following extra conditions can be derived:

$$\left(\overline{\overline{Z}}_{\rm se}\right)^T = \overline{\overline{Z}}_{\rm se}, \tag{3a}$$

$$\left(\overline{\overline{Y}}_{\rm sm}\right)^T = \overline{\overline{Y}}_{\rm sm}, \tag{3b}$$

$$\begin{bmatrix} K_{xx,\rm me} & K_{xy,\rm me} \\ K_{yx,\rm me} & K_{yy,\rm me} \end{bmatrix} = \begin{bmatrix} -K_{yy,\rm em} & K_{xy,\rm em} \\ K_{yx,\rm em} & -K_{xx,\rm em} \end{bmatrix} \tag{3c}$$

where T stands for the transpose operation and $K_{kl,\rm me/em}$ $(k, l \in \{x, y\})$ are the elements of the respective coupling coefficient tensors.

Combining (1) and (2), we arrive at a set of expressions that connect the tangential electric and magnetic fields at the two sides of the boundary through the HMS parameters,

$$\frac{1}{2}\left(\mathbf{E}_{t,1} + \mathbf{E}_{t,2}\right) = \overline{\overline{Z}}_{\rm se} \cdot (\hat{\mathbf{n}} \times (\mathbf{H}_2 - \mathbf{H}_1)) - \overline{\overline{K}}_{\rm em} \cdot \left[\hat{\mathbf{n}} \times (-\hat{\mathbf{n}} \times (\mathbf{E}_2 - \mathbf{E}_1))\right], \tag{4a}$$

$$\frac{1}{2}\left(\mathbf{H}_{t,1} + \mathbf{H}_{t,2}\right) = \overline{\overline{Y}}_{\rm sm} \cdot (-\hat{\mathbf{n}} \times (\mathbf{E}_2 - \mathbf{E}_1)) + \overline{\overline{K}}_{\rm me} \cdot \left[\hat{\mathbf{n}} \times (\hat{\mathbf{n}} \times (\mathbf{H}_2 - \mathbf{H}_1))\right]. \tag{4b}$$

The first design step of a HMS includes determining the HMS parameters $\overline{\overline{Z}}_{\rm se}$, $\overline{\overline{Y}}_{\rm sm}$, $\overline{\overline{K}}_{\rm em}$, $\overline{\overline{K}}_{\rm me}$ for a desired wave transformation. Then, the required profiles are discretized and realized by means of appropriately engineered unit cells, as described in Section III.

Although the first demonstrated HMSs were non-bianisotropic (i.e., $\overline{\overline{K}}_{\rm em} = \overline{\overline{K}}_{\rm me} = 0$), it was soon realized that bianisotropy offers another degree of freedom by coupling the electric and magnetic responses, as evident from (2). Two types of bianisotropy are particularly interesting for the applications discussed in this paper: Omega-bianisotropy and chirality. In the case of Omega-bianisotropic Huygens' metasurfaces (O-BHMSs), the coupling coefficients

$\overline{\overline{K}}_{\rm em}$, $\overline{\overline{Z}}_{\rm me}$ have diagonal nonzero elements. Then, provided that the tensors $\overline{\overline{Z}}_{\rm se}$, $\overline{\overline{Y}}_{\rm sm}$ are also diagonal, the boundary conditions presented in (4) can reduce to a scalar form for each polarization (transverse electric or transverse magnetic) and the HMSs are characterized as scalar [15]. In a physical interpretation, Omega-bianisotropy refers to the scenario that the induced electric (magnetic) currents remain orthogonal to the acting magnetic (electric) fields. This type of electromagnetic coupling was proven essential to overcome limitations observed in the early demonstrations of non-bianisotropic scalar HMSs, such as the transmission efficiency drop for wide-angle anomalous refraction [16]. On the other hand, in chiral metasurfaces the induced electric (magnetic) currents are parallel to the acting magnetic (electric) fields, meaning that the tensors $\overline{\overline{K}}_{\rm em}$, $\overline{\overline{K}}_{\rm me}$ have off-diagonal nonzero elements. This type of bianisotropy is essential to design HMSs for chiral polarization effects, such as polarization rotation or circular polarization selectivity [17]–[19].

In most practical applications, it is required that the designed HMSs are passive and lossless. Losses would reduce the efficiency of the structures, while active regions across the HMSs would significantly complicate their physical realization. Therefore, it is important to arrive at sufficient conditions for the input and output fields of a passive and lossless HMS. For O-BHMSs it has been proven in [15] that any Maxwellian wave transformation is feasible with a passive and lossless design, if the real part of the power density normal to the metasurface is locally conserved, i.e.,

$$\frac{1}{2}\mathrm{Re}\left\{\hat{\mathbf{n}}\cdot(\mathbf{E}_2\times\mathbf{H}_2)\right\}=\frac{1}{2}\mathrm{Re}\left\{\hat{\mathbf{n}}\cdot(\mathbf{E}_1\times\mathbf{H}_1)\right\} \qquad (5)$$

Under the satisfaction of the local power conservation condition in (5), the parameters of $Z_{\rm se}$, $Y_{\rm sm}$, $K_{\rm em}$ of a scalar O-BHMS can be uniquely defined based on the electric and magnetic fields at the two sides of the boundary [15], Eq. (5)]. After discretizing the HMS, the response at each unit cell can then be modeled through an impedance matrix Z or a generalized scattering matrix S with their elements given as a function of $Z_{\rm se}$, $Y_{\rm sm}$, $K_{\rm em}$ at each sampling point [15], [20]. In other design scenarios, such as chiral HMSs, it may be more convenient to directly define lossless scattering matrices without going through the formulation involving the tensors $\overline{\overline{Z}}_{\rm se}$, $\overline{\overline{Y}}_{\rm sm}$, $\overline{\overline{K}}_{\rm em}$, $\overline{\overline{K}}_{\rm me}$ [18], [19]. Lastly, it should be emphasized that the physically realized unit cells inevitably suffer from copper and dielectric losses. However, by trying to approximate the scattering matrix of the ideal lossless design for each unit cell, the losses are minimized, and the desired functionality of the HMS is achieved.

III. METASURFACE REALIZATION AND UNIT CELL DESIGN

In the previous sections, the theoretical framework for deriving a set of boundary conditions for controlling arbitrary transformations of electromagnetic waves was detailed. Specifically, by utilizing a set of current densities, both electric and magnetic, complete control over desired field transformations could be obtained [9]–[11]. Furthermore, by employing a combination of electric impedance, magnetic admittance, and magnetoelectric coupling tensors, a method of exciting the required current densities without impressed sources became possible. However, while these surface's constitutive properties are straightforward to obtain theoretically, realizing a physical structure can still be challenging. The standard method of physically representing these surface parameters is to first discretize the continuous boundary conditions. The discretized boundary values are then represented utilizing electrically small scatterers known as 'unit cells' or 'meta-atoms' [9]–[11]. These unit cells or meta-atoms then serve as the building blocks for realizing a metasurface. By designing and tuning the scattering characteristics of these unit cells, the desired electromagnetic properties of these structures can be obtained. Assembling arrays of the designed unit cells, the desired metsurface can be realized with the stipulated functionality.

The inherent characteristic of a metasurface unit cell which allows an accurate representation of a set of desired boundary conditions, is their electrically small and usually sub-wavelength size. As compared to transmit- and reflect-array unit cells, which are often around half wavelength in their lateral dimension, metasurface unit cells are typically much smaller in size, often ranging from a sixth to a tenth of the operating wavelength in their lateral dimensions [9], [11], [21]–[24]. Due to their extremely sub-wavelength nature, metasurface unit cells allow homogenization of their electrical properties. Such homogenization and electrically small size allow them to accurately realize the continuous boundary conditions presented in Eqs. (4). Furthermore, their small size also naturally suppresses issues with undesired coupling effects in both the longitudinal direction through the unit cell and the lateral direction with neighboring cells. These combined effects give metasurface unit cells more intimate control of their scattering properties as compared to their transmit- and reflect-array counterparts.

In recent years, as the functionality and applications of metasurfaces have advanced, so have the design and realization of metasurface unit cells. Designs including stacked layer cells, wire-loop cells, omega-shaped inclusions, spiral-shaped inclusions, among many others have been demonstrated [9], [20]–[22], [25]–[32]. Examples of such unit cells and meta-atoms can be seen in Fig. 2, which include single polarization unit cells as seen in Fig. 2(a) and Fig. 2(b) as well as tensorial unit cells for polarization control in Fig. 2(c) and Fig. 2(d). While any sub-wavelength scatterer may be utilized as a unit cell, there have been two prevailing topologies utilized in recent years, namely the stacked-layer and wire-loop structures. In the following sections, discussions and examples of these two popular topologies will be detailed.

A. STACKED-LAYER UNIT CELL TOPOLOGY

The stacked-layer unit cell is one of the most recognizable and utilized unit cell topology. These structures are constructed

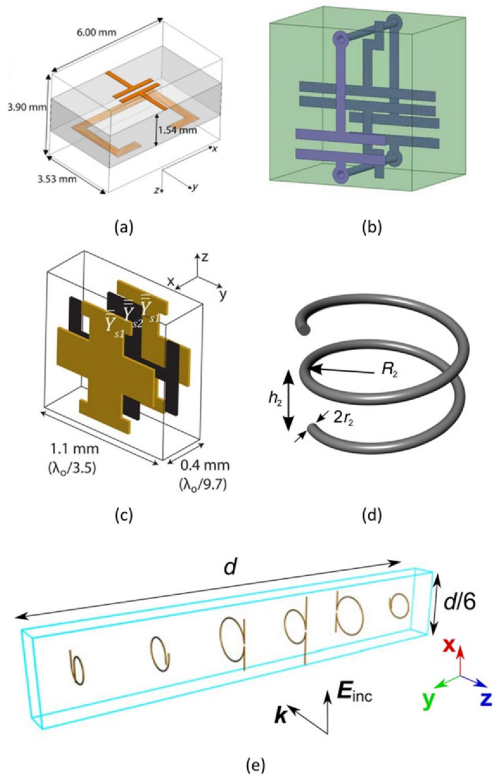

FIGURE 2. Examples of metasurface unit cells. (a) Transverse wire-loop unit cell [9]. (b) Longitudinal wire-loop unit cell [21]. (c) Three stacked-layer unit cell [28]. (d) Helix-shaped inclusion [27]. (e) Omega-shaped inclusion [26].

by stacking multiple substrates together with etched metal features [20], [22], [32]. Typically, by tuning the metal geometries, different scattering characteristics of the unit cells can be obtained. Although the theoretical boundary conditions indicate the requirement for both electric and magnetic responses, the stacked-layer unit cell uses a combination of multiple metal scatterers to achieve both effective electric and magnetic properties. One aspect of the stacked-layer unit cell is the number of layers that is needed to realize a certain desired response. In general, with negligible layer-to-layer coupling, three layers, specifically three metal layers on two bonded substrates, are sufficient to realize any desired single polarization unit cell response [10], [16]. The design of stacked-layer unit cells typically involves utilizing a transmission-line model, which models the substrates as transmission-line segments and the etched metal layers as lumped shunt admittance or impedance elements [10], [16]. By matching the equivalent transmission-line model of the unit cells to the desired boundary conditions, the required shunt admittance or impedance values of their circuit model can be obtained. Suitable metal geometries which realize these shunt admittance or impedance values could then be explored and designed to realize a physical unit cell. As there are no restrictions on the possible metal geometries, a myriad of layer structures have been utilized in recent years including meander lines, Jerusalem crosses, dog bones, among others [20], [22], [23], [28], [32]. Although coupling between neighboring unit cells cannot be captured, while designing each of them individually, it is generally low and does not affect the accuracy of the realized transformations. However, in cases that coupling is nontrivial, global post-optimization could be performed using full-wave CAD tools to adjust for this intercell coupling. Alternatively, walls acting as baffles and realized using vias can be used between the unit cells to further decouple them [24].

For the first realizations of stacked-layer unit cells for metasurfaces, the utilized unit cells were typically symmetric. However, as it was seen with applications such as wide-angle refraction, such symmetric unit cells could not produce reflectionless, lossless, and passive designs [15], [33]. This issue arose due to the impedance mismatch of the incident and refracted waves [16]. To resolve this issue, Omega-bianisotropy was utilized. Additionally, to realize this Omega-bianisotropy, the asymmetric stacked-layer unit cell was proposed. In essence, by utilizing asymmetry in the unit cell design, matching of different impedances for the input and output of the unit cell became possible [16]. Although the asymmetric stacked-layer unit cell was not the first topology to demonstrate Omega-bianisotropy, they provide a much simpler method of realizing O-BHMSs with standard printed circuit board (PCB) fabrication technologies.

It should also be mentioned that although three layers are typically sufficient for most desired responses, additional layers may add to improved functionalities of the unit cells. One area where such effect is greatly notable is in reducing the unit-cell losses. In three stacked-layer unit cells, it has been noticed that high resonant losses in the metal layers were often observed [20], [23]. However, such issues may be alleviated when using additional number of layers, at the cost of increased fabrication difficulty and design complexity. Depending on the desired application, the four stacked-layer unit cell may prove to be more appropriate as compared to the three stacked-layer design.

B. WIRE-LOOP UNIT CELL TOPOLOGY

While the stacked-layer topology is more frequently utilized, the wire-loop unit cell topology can be regarded as a more direct and natural implementation of the boundary conditions. As a set of both electric and magnetic currents are required to achieve arbitrary wave transformations, a wire-loop structure is able to represent these currents directly [9], [21], [34]. Specifically, an electric wire serves to produce and control the desired electric current, while an electric loop controls an effective orthogonal magnetic current. By combining the scattered fields from these two structures, the wire-loop unit cell is able to directly realize a Huygens' source. Due to this property, some of the earliest demonstrations of metasurface designs utilized the wire-loop topology, such as with the refractive designs shown in [9], [21].

It should also be mentioned that there are different ways in which the wire-loop unit cell can be realized. One such method is to utilize transverse designs where both the electric

wire and the loop are etched on a single substrate such as with the example shown in Fig. 2(a) [9]. However, to align the direction of the electric and magnetic dipole moments with the wire and loop, cuts of the metasurface need to be placed in a stacked manner [9], [34]. Unfortunately, such complicated assembly can lead to increased difficulties of realizing such designs. A second method is to use a longitudinal wire-loop design, where metallized vias through substrates are used to form the electric loop as seen in Fig. 2(b) [21]. In the longitudinal wire-loop design, post fabrication assembly of the metasurface is not required. However, the required vias increase the fabrication difficulties of the design. While both topologies are capable of realizing metasurfaces, depending on their respective trade-offs, they may be suited for different applications.

The examples in Fig. 2(a) and Fig. 2(b) were the first generation of wire-loop unit cell designs. Specifically, these unit cells were non-bianisotropic. As discussed previously, bianisotropy can lead to remarkable effects such as polarization and asymmetric matching with chirality and Omega-bianisotropy respectively. Thus, as exploration of bianisotropic metasurface applications expanded, Omega-bianisotropic versions of the wire-loop topology also emerged [34], [35]. As discussed with the stacked-layer topology, it was shown that asymmetry of the unit cell can be utilized to realize Omega-bianisotropy. Using the same asymmetry approach, asymmetric transverse wire-loop unit cell designs were also shown to achieve Omega-bianisotropy. Functionalities of dielectric matching and wide-angle reflection-less refraction were demonstrated with such designs [34], [35].

It should also be discussed that like the stacked-layer topology, equivalent circuits have been utilized to analyze the performance of the wire-loop unit cell. Namely, lattice networks have been shown to model the wire-loop unit cells intimately for both non-bianisotropic and Omega-bianisotropic HMS designs [35]. Due to the possible wide-band nature of the lattice network, the wire-loop unit cells have also been shown to be wide band and in theory could be engineered to achieve an all-pass response [35].

IV. APPLICATIOS OF HUYGENS' METASURFACES

A. 'PERFECT' REFRACTION

One of the earliest demonstrations of metasurfaces involved arbitrary refraction of electromagnetic fields. More specifically, 'perfect' or reflectionless refraction was desired. It is well known that for refraction between two media, there exists a remarkable effect known as the Brewster angle, where transverse magnetic (TM) waves refract between dielectric media without any reflections. However, this effect only exists for one single angle of incidence depending on the material properties of the two media, and for all other angles of incidence, reflections are always present. Fortunately, due to the ability of metasurfaces to produce arbitrary wave transformations, a method of perfect refraction with tailored incident and refracted angles becomes possible. The first demonstrations of refraction were achieved with symmetric wire-loop unit cells as seen in [9], [21]. These designs realized non-bianisitropic boundary conditions and were able to demonstrate the desired refraction with negligible reflections utilizing passive and lossless structures.

While both demonstrations showed promise for refractive functionalities, it also became apparent that such designs would not be feasible for wide-angle refraction. As previously mentioned, this was due to the impedance mismatch of the incident and refracted waves [16]. At shallow angles of refraction (assuming normal incidence), the impedance mismatch would be minimal which allowed these symmetric designs to suffer negligible reflections. However, as the desired refraction angle was increased, the impedance mismatch issue was exacerbated, and such symmetric structures no longer could achieve reflectionless transformations. This issue was also investigated theoretically, which revealed that non-bianisotropic designs cannot simultaneously produce lossless, passive, and reflectionless transformations for different input and output wave impedances. Due to this issue, any passive non-bianisotropic designs, as in the case with the symmetric wire-loop metasaurfaces, would inevitably experience increased reflections for wide-angle refraction.

To alleviate this issue, Omega-bianisotropy was utilized. Through demonstration via both microwave network and full field theory approaches, it was revealed that Omega-bianisotropy would allow perfect matching of arbitrary input and output impedances, even for passive and lossless designs [15], [16]. Additionally, such Omega-bianisotropy could be physically realized through asymmetry of the unit cell design. Demonstrations of such Omega-bianisotropy refraction designs were first presented for the asymmetric stacked-layer unit cell [20], [32]. Through both full-wave simulations and measurements, negligible reflections were observed for extreme angles of refraction.

Following demonstrations of 'perfect' wide-angle refraction with stacked-layer designs, Omega-bianisotropic wire-loop unit cells were also shown to be capable of achieving the same desired refraction [34]. Similar to their stacked-layer counterparts, the Omega-bianisotropic wire-loop metasurface also achieved negligible reflections and wide-angle refraction with comparable scattering refraction efficiency. Measurement results for the above mentioned wire-loop wide-angle refraction design around 21 GHz can be seen in Fig. 3 and Fig. 4

As shown in Fig. 3(b) the specular reflections of the metasurface centered at 21.6 GHz, which was characterized in a quasi-optical setup shown in Fig. 3(a), demonstrated negligible specular reflection, as desired. Additionally, the refractive nature of the metasurface was characterized through a far-field antenna measurement setup by placing the metasurface in front of a receiving horn antenna. By measuring the horn antenna with the metasurface as an overall antenna under test (AUT), the radiation profile of the composite system was obtained. As seen in Fig. 4, the measured radiation pattern demonstrated that the metasurface is able to refract the

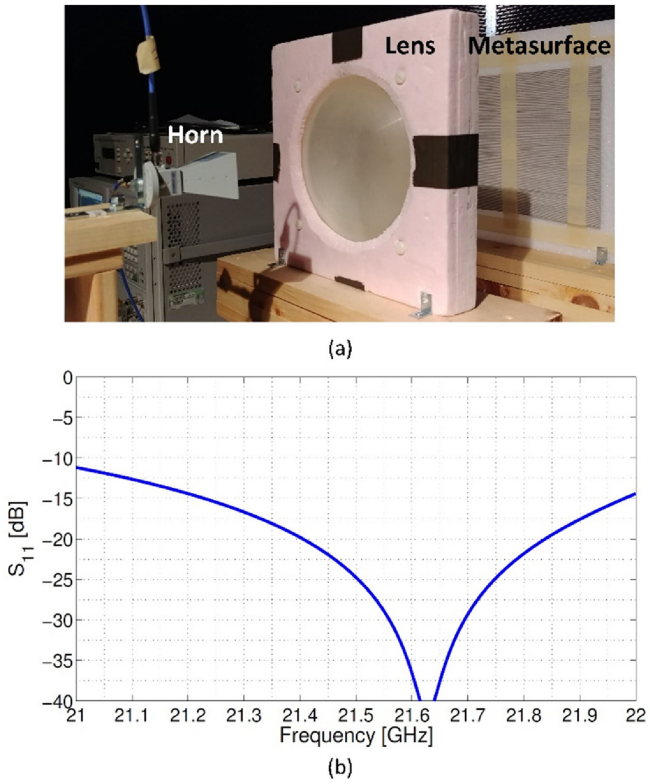

FIGURE 3. Reflection setup and measurement of Omega-bianisotropic wide-angle refraction metasurface [34]. (a) Quasi-optical measurement setup including horn antenna, lens for collimation, and metasurface under test. (b) Measured specular reflection of metasurface with a center frequency of 21.6 GHz.

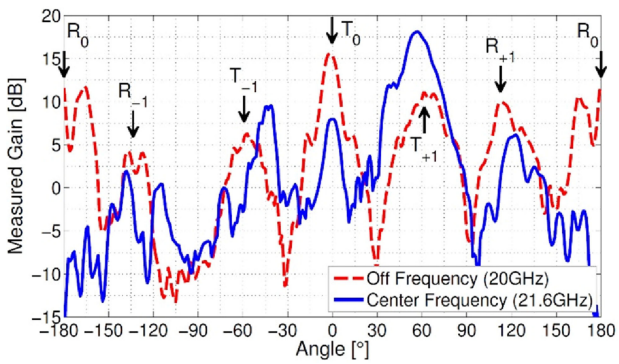

FIGURE 4. Measured realized gain of Omega-bianisotropic wide-angle refraction Huygens' metasurface placed in front of a receiving horn in a far-field anechoic antenna test measurement setup at the center frequency of 21.6 GHz and off center frequency at 20 GHz, with the possible Floquet modes for both transmission (T_{+1}, T_{-1}, and T_0) and reflection (R_{+1}, R_{-1}, and R_0) regimes indicated [34].

normally incident radiation of the horn antenna to an extreme angle at the center frequency of 21.6 GHz. Through analysis of the measured results, the metasurface demonstrated a scattering refraction efficiency of 80%, denoting that 80% of the scattered power was coupled to the desired refraction direction. Such scattering efficiency would not be possible with non-bianisostropic designs for the same desired angle of refraction. As Fig. 4 shows, at the correct frequency, all possible propagating Floquet modes are suppressed which is a remarkable feature of Huygens' metasurfaces. The designs in [20], [32], [34] demonstrated the ability for realizing Omega-bianisotropic Huygens' metasurfaces with standard PCB fabrication techniques and achieving improved performance as compared to previous non-bianisotropic designs.

B. THIN LENSES

One of the most sought-after applications of metasurfaces is for the enhancement of antenna systems, specifically metasurface lenses for enhancing the gain of a feed antenna. Microwave lenses have been commonly used for collimation of antenna patterns. However, these traditional lenses are often manufactured by shaping dielectric materials. Due to their size and volume, dielectric lenses are often heavy and bulky. Additionally, reflections due to the mismatch of air and the dielectric lens can often produce undesired effects. To alleviate these issues while still providing the benefit of utilizing a lens to enhance antennas, metasurface lenses have been employed. Due to the thin and flat profile of metasurfaces, these lens designs are made to be sleek and lightweight. Additionally, by controlling the electrical properties of these designs, reflections can be controlled and minimized. Although metasurface lenses are thin, they are designed to still provide the collimating functionality that is desired with traditional dielectric lenses.

Metasurface lenses are often compared to transmit-arrays which may share similar functionalities. However, there are fundamental differences between the two design regimes. The standard method of designing transmit-arrays is to encode a modulated phase profile into the transmitting surface structure. The desired phase is often obtained through ray-tracing from a feeding antenna to the surface. Metasurfaces on the other hand, utilize full field quantities to realize the desired boundary conditions [36]. Due to the utilization of full field quantities, metasurface have improved control over reflections and the excitation of higher order Floquet modes, which transmit-arrays often lack [36]. In the case of Omega-bianisotropic designs, Huygens' metasurface lenses may even be made completely reflectionless, which is not achievable with traditional transmit-array designs. Such design considerations become increasingly important for lens designs with small F/D (focal length / diameter) ratios, where the lens may be placed close to the source antenna and control over reflections becomes necessary.

An example of a TM metasurface collimating lens can be seen in Fig. 5 [23]. The lens is centered around 34.3 GHz with a bandwidth of 1.8 GHz. At the center frequency, the lens has a focal length of 3λ and a diameter of 15λ, resulting in a small F/D ratio of 0.2. The lens is designed to increase the gain of a feeding slotted waveguide antenna (SWGA). The waveguide antenna radiates through a row of slots 40λ in length at 34.3 GHz. Additionally, the waveguide antenna scans between −20° to broadside within the operational band via frequency scanning. The metasurface lens is then designed

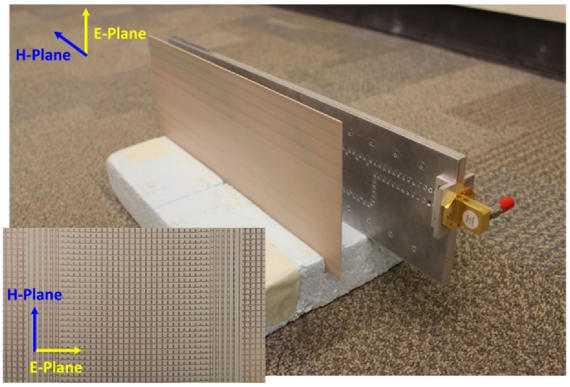

FIGURE 5. **Huygens' metasurface lens with slotted waveguide antenna, with zoomed inset in region of the metasurface [23].**

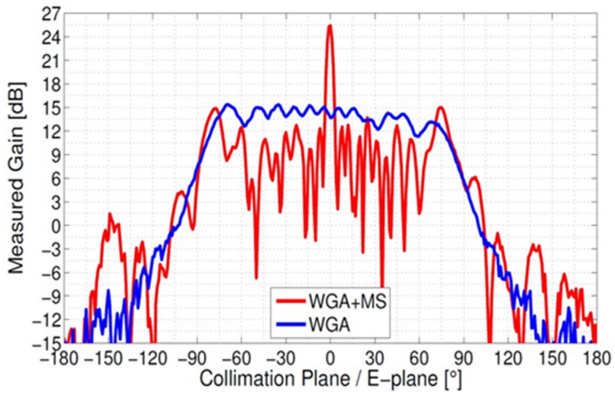

FIGURE 6. **Measured realized gain of the slotted waveguide antenna with (SWGA+MS) and without the Huygens' metasurface lens in the collimation plane [23].**

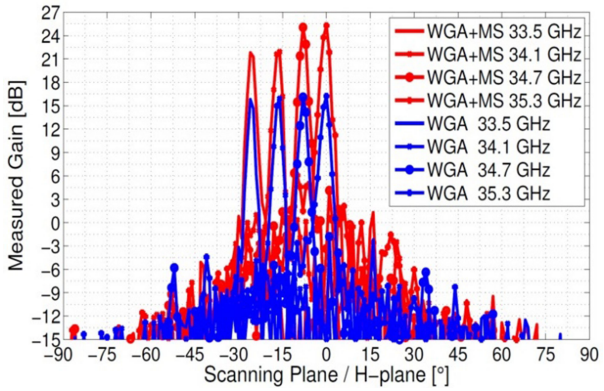

FIGURE 7. **Measured realized gain of the waveguide antenna with (SWGA+MS) and without the metasurface lens in the scanning plane for the scan range of −20° to broadside [23].**

to provide gain enhancement throughout the entire band of operation without disturbing the scanning capability of the SWGA. The overall antenna system comprising the metasurface lens and the SWGA can be seen in Fig 5.

The measured gain enhancement of the Huygens' metasurface lens can be seen in Fig. 6 and Fig. 7. In Fig. 6, the measured gain of the SWGA with and without the metasurface in the collimation plane can be seen. As shown, the metasurface is able to collimate the wide radiation pattern of the SWGA and produce a collimated beam. The result of this collimation is experienced as an increase of the realized gain. Additionally, as the SWGA scans, the Huygens' metasurface lens was able to continuously increase the output antenna gain without disturbing the scanning capability. As shown in Fig. 6, depending on the scanning angle, the passive metasurface lens was able to provide upwards of 10 dB of increased realized gain.

Aside from collimation, Huygens' metasurface lenses may also be utilized for other applications, such as extending the scan range of antenna arrays. As discussed in [37], a diverging Huygens' metasurface lens placed in the far-field of a phased array may provide continuous angle doubling or tripling to the overall antenna system. Such functionalities could lessen the scanning requirement of the feed antenna, which may significantly reduce the overall design complexity and cost of antenna systems.

C. POLARIZATION CONTROL

Controlling the polarization states of electromagnetic (EM) waves is another important aspect in many practical applications such as satellite communications and imaging systems. While birefringence can be adopted in the design of a metasurface, it offers limited polarization control in the sense that it fails to manipulate the flow of different circular polarizations (CPs). In this regard, chiral metasurfaces have attracted much interest as they offer more advanced functionalities such as CP sessslectivity and polarization rotation. To date, various chiral metasurfaces have been reported which are mainly realized by (i) utilizing chiral bianisotropic meta-atoms whose induced electric (magnetic) dipole moments are in parallel with the acting magnetic (electric) field, and (ii) cascading anisotropic electric impedance sheets.

To conceptually visualize the working principle behind the first method, we discuss how chiral bianisotropic meta-atoms can be used to realize a circular polarization selective surface (CPSS). A CPSS is a type of chiral surface which transmits one handedness of CP while reflecting the opposite handedness. For this purpose, consider a metasurface formed by an array of chiral bianisotropic meta-atoms (e.g., metallic helices) that are oriented along the z-axis. If an acting electric field is polarized along the z-axis, the electric dipole moments are induced along the z-axis due to the orientation of the meta-atoms. Additionally, the acting electric field would also induce parallel magnetic dipole moments along the z-axis as the meta-atoms are assumed to possess chirality. These two induced electric and magnetic dipole moments radiate orthogonal electric fields since the z-oriented electric dipoles radiate electric fields that are polarized in the θ direction, while the z-oriented magnetic dipoles produce electric fields in the ϕ direction. As such, provided that these two parallel dipole moments generate the fields that are of equal magnitude but out of phase by 90°, the metasurface essentially functions as an

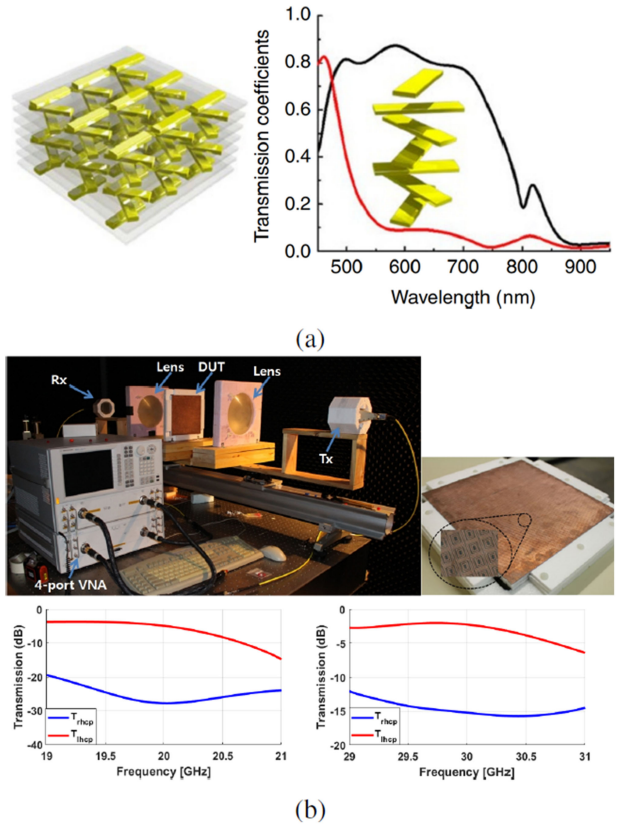

FIGURE 8. **(a) Left: A schematic of a twisted-metamaterial polarizer comprising cascaded arrays of gold nanorods that are rotated with respect to one another. Right: Transmission coefficients of CP waves with two opposite handedness (red and black curves respectively correspond to left-handed and right- handed CP waves) Reprinted figure from [38]. (b) Top: Experimental set-up used for characterizing the dual-band CPSS in [18]. Bottom Left: The measured transmission coefficients (in dB) of CP waves for two opposite handedness near 20 GHz (red and blue curves respectively correspond to right-handed and left-handed CP waves). Bottom Right: The measured transmission coefficients near 30 GHz. Reproduced figure from [18].**

ideal CPSS. Based on such an idea, the authors in [17] demonstrated various chiral polarization control functions with an array of helical meta-atoms.

In departure from explicitly utilizing nonzero magnetoelectric coupling coefficients, chiral effects can also be achieved by cascading anisotropic layers that only possess electric responses (i.e., $\overline{\overline{Z}}_{se}$). For example, Zhao *et al*. have captured much attention with their initial proposal of a 'twisted-metamaterial' in which they demonstrated CP selectivity by cascading an array of rotated gold nanorods [38]. In these twisted-metamaterials (Fig. 8(a)), the gold nanorods do not possess any intrinsic chiral response, but the chirality is induced from the progressive rotation of the nanorods along the propagation direction of an incident wave (i.e., the rotated lattice effect) [39]. The efficiency of the demonstrated CPSS, however, was not necessarily close to unity because the impedance-matching condition was not guaranteed to be satisfied for the transmitted CP field. Subsequent work by Selvanayagam and Eleftheriades resolved this issue by cascading two non-bianisotropic HMSs [40]. In particular, these authors obtained chiral effects by rotating the HMSs with respect to one another similar to the twisted-metamaterials. On the other hand, they allowed the off-diagonal elements of $\overline{\overline{Z}}_{se}$ and $\overline{\overline{Y}}_{sm}$ for their non-bianisotropic HMSs to be nonzero to precisely control the reflection, thereby satisfying the impedance-matching condition. Following this work, the same authors demonstrated chirality with minimal number of anisotropic layers that possesses purely electric responses (3 layers for CPSSs and 4 layers for polarization rotators) [41]. In particular, the authors utilized the multi-conductor transmission line (MTL) theory to precisely determine the required anisotropic impedance values in each layer and demonstrated general chiral properties with minimal number of layers, while maximizing efficiency. The proposed systematic method was further developed by Kim and Eleftheriades where they combined the MTL theory with a nonlinear optimization technique to experimentally demonstrate a dual-band chiral metasurface [18] (Fig. 8(b)).

In [19], the idea of cascading anisotropic electric layers for realizing a chiral metasurface was further expanded by also combining wavefront engineering capabilities. In particular, the authors incorporated the theory of Pancharatnam-Berry phase shift in the design of a CPSS to selectively apply a phase shift only for the reflected CP wave, while preserving the impedance-matching condition for the opposite handedness. Four tensor impedance layers were cascaded and twisted with respect to one another to acquire the necessary chiral effects, while individual meta-atoms were rotated once more to induce the geometric phase shift (i.e., the Pancharatnam-Berry phase shift). In this sense, the authors used two rotations: (i) a rotation of each anisotropic electric layer for producing chirality and (ii) another rotation of individual meta-atoms for obtaining the geometric phase shift as shown in Fig. 9(a). Their experimental setup and the results are shown in Fig. 9(b) from which it is seen that the left-handed CP field is reflected at 33° off broadside, while the right-handed CP field is transmitted with minimal reflection. Following this work, Kazemi *et al*. numerically demonstrated refraction of a plane wave, while rotating its polarization angle by 90° [42].

Whereas the discussion thus far focused around CPSSs that reflect one handedness of CP while transmitting the opposite handedness, it should be briefly mentioned that CP selectivity can also be achieved by utilizing unequal Ohmic losses in the metasurface for two orthogonal CP waves (i.e., circular dichroism). Chiral metasurfaces that rely on circular dichroism typically consist of asymmetric unit cells whose resonant modal profiles are different for two orthogonal CP waves [43], [44]. This difference allows the incident left- and right-handed CP waves to perceive different absorption coefficients, thereby producing a non-zero circular dichroism. Nevertheless, similar to the early CPSSs that reflect/transmit particular CP waves, their chiral dichroism in transmission is typically not unity due to the explicit utilization of Ohmic losses which inevitably impacts the transmission for both CP waves and fails to satisfy the impedance-matching condition.

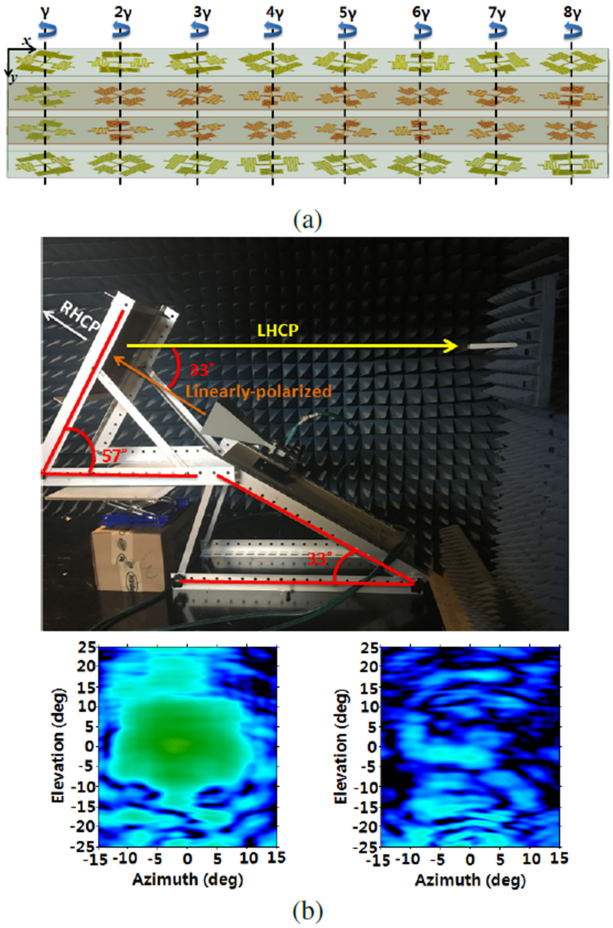

FIGURE 9. **(a) An array of the phase-gradient CPSS in [19]. (b) Top: Experimental set-up used for characterizing the phase-gradient CPSS. Bottom Left and Right: The measured far-field amplitude distribution for the reflected left-handed CP field (left) and right-handed CP field (right). Reproduced figure from [19].**

D. BEAMFORMING

Huygens' metasurfaces have demonstrated general beamforming capabilities that can be utilized to synthesize antenna patterns without resorting to conventional antenna arrays. In such antenna systems, one or more HMSs transform the electromagnetic radiation of a single source into the necessary aperture fields corresponding to desired radiation patterns in the far-field. Therefore, the use of metasurfaces eliminates the requirements for complex feeding networks of the array elements that can increase the fabrication cost and limit the power efficiency due to losses. Although the local power conservation condition in (5) seems constraining in the case of prescribed incident fields and a desired output aperture, different ways have been proposed in the literature to achieve highly efficient beamforming with a single source. These include redistributing the power and restoring the local power density matching by use of a cavity-excited HMS [25], [45], [46], pairs of HMSs [47]–[49] or auxiliary surface waves [50].

Cavity-excited HMS were first demonstrated in [25], where a highly-directive beam was produced with a low-profile

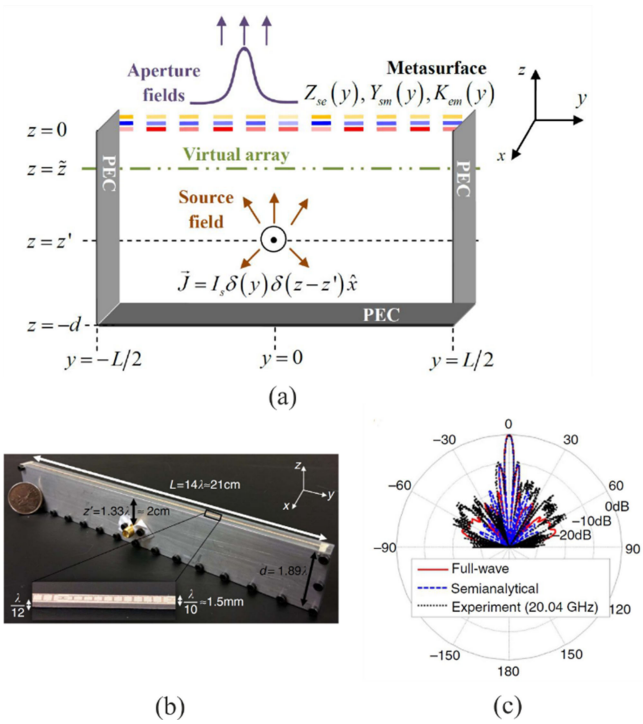

FIGURE 10. **Cavity-excited HMS for beamforming applications [25], [45]. (a) Schematic of the structure, (b) Fabricated cavity-excited HMS for highly-directive radiation towards broadside [25], (c) Simulated, theoretical and measured radiation patterns.**

single-fed cavity. Specifically, a HMS was placed at the open side of an orthogonal metallic cavity, as seen in Fig. 10(a). The electromagnetic fields within the cavity take the form of lateral cavity modes that exhibit multiple reflections between the perfect electric conductor (PEC) base of the cavity and the metasurface. It was shown that coupling to the higher-order (propagating) lateral modes is required for maximum directivity due to the better illumination of the aperture and the suppression of grating lobes. Because the HMS in [25] was non-bianisotropic, the reflected and transmitted fields were constrained not only by the local power conservation condition in (5), but also by the requirement of equal wave impedances at the two sides of the HMS. However, by optimizing the height d of the cavity and the position z' of the source, it was possible to couple most of the input power to the highest-order lateral modes and achieve a highly-directive beam at the output. A design of length $L = 14\lambda$ (where λ is the free-space wavelength for a frequency at 20 GHz) was fabricated with the HMS consisting of 'spider-type' unit cells. The simulated and measured aperture illumination efficiency was 86 % and 75 %, respectively. In addition, the measured and simulated radiation patterns showed good agreement with the semi-analytically predicted one, as shown in Fig.10(c).

In [45] the concept of cavity-excited HMS was expanded by considering Omega-bianisotropic HMSs on the top of the cavity. The extra degree of freedom allows to have full control of the amplitude and phase of the output fields and, thus, realize prescribed antenna patterns. The output fields are determined

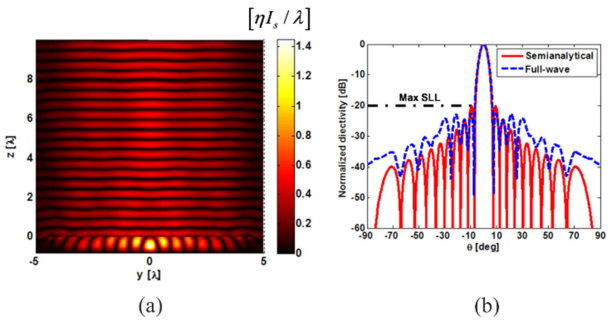

FIGURE 11. Cavity-excited HMS for beamforming applications [45]. (a) Real part of the electric field |Re{E_x}| as obtained from full-wave simulations for a desired Taylor output aperture, (b) Theoretical and simulated radiation patterns.

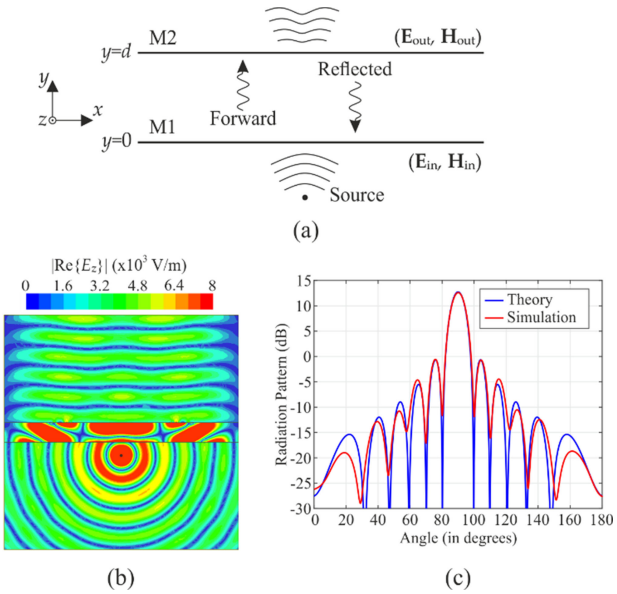

FIGURE 12. Huygens' metasurface pairs for non-local power conserving transformations [49]. (a) Schematic of the structure, (b) Real part of the electric field |Re{E_z}| as obtained from full-wave simulations for a desired uniform output aperture and a separation distance $d = 0.5\lambda$ between the two HMSs, (c) Theoretical and simulated radiation patterns.

based on the desired radiation characteristics using the "virtual array" method. Specifically, an array of Huygens' sources having currents according to the desired antenna design (e.g., Taylor antenna, Chebyshev array antenna) is conceptualized at a plane $z = \tilde{z}$ below the HMS and the output aperture fields are calculated as the fields emitted by the virtual array sources at the plane $z = 0$ [Fig. 10(a))]. By reasoning of the equivalence principle, these aperture fields, if established at the output of the HMS, will produce the desired far-field radiation pattern.

The fields within the cavity in [45] were also analyzed in a summation of lateral cavity modes. In order to arrive at a passive and lossless design, the reflection coefficients from the HMS for each lateral mode and the position of the source were optimized, so that the total input and output fields minimize the local power mismatch at the boundary. Once the optimization was converged, the Omega-bianisotropic HMS was modeled using the three-impedance layers approach, as described in Section III. Different Taylor aperture antenna patterns were demonstrated with high accuracy in terms of the radiation characteristics, as observed in Figs. 11(a)–11(b). Moreover, given that the HMS is the only open side of the cavity, there were not any leakage losses and the power efficiency drop in a physical implementation would only be attributed to the losses of the HMS and the walls of the cavity.

An alternative approach for general antenna beamforming is the use of pairs of Omega-bianisotropic HMSs, as sketched in Fig. 12(a). The fields at the input of the metasurface pair ($y = 0^-$) are calculated based on the electromagnetic source, while the output fields of the HMS pair ($y = d^+$) are determined from the desired radiation pattern. As explained before, the main constrain in this case is the local power conservation requirement that should be satisfied for passive HMSs, even if bianisotropy is present. However, by allowing the wave to propagate for a distance d between the two HMSs, it is possible to redistribute the power density profile. Therefore, for appropriate electric and magnetic fields in the region between the two metasurfaces, it is possible to achieve local power conservation for each metasurface individually, while the input and output power profiles of the total structure are different. Although the sides of the structure are left as open boundaries, by equating the total incident and output power, the power leakage at the sides is minimized.

Naturally, the above-described problem reduces to calculating the fields in the region $0^+ < y < d^-$ that satisfy: (a) Maxwell equations, and (b) the power-density boundary conditions defined by the local power conservation requirements at the two HMSs. Due to the complexity of the problem, all proposed solutions resort to some kind of optimization that minimize the total local power mismatch at the two boundaries. In [47], a phase-retrieval algorithm was employed to find the appropriate phase profile that the fields should acquire from M1, so that the power density profile at the input of M2 is the desired one. On the other hand, in [48] the fields at the output M1 were expanded in a set of basis functions with unknown complex weights. By carefully employing Maxwell's equations to propagate the field distribution, the power density profiles were calculated at the inner boundaries of the two HMSs as a function of the unknown weights. Subsequently, a power-based point-matching process was utilized to acquire a nonlinear system of equations, which was then solved with standard optimization techniques. The latter method, inspired by the Method of Moments formulation, was further expanded in [49] to accommodate for the case that the source is placed within the metasurface pair. The use of multiple reflections between the two HMSs was also studied as a promising way to reduce the required separation distance and design more compact structures. Numerous nonlocal power conserving transformations were demonstrated with HMS pairs, as for example, the conversion of the cylindrical wave of a single current line source to a uniform output aperture. The use of multiple

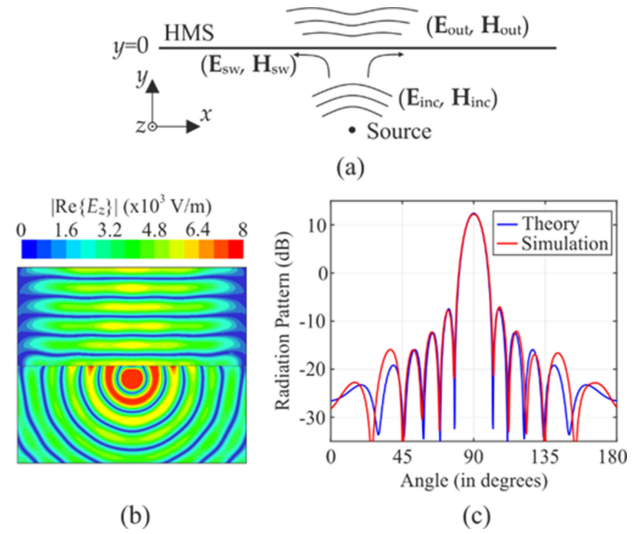

FIGURE 13. A single Omega-bianisotropic HMS for non-local power conserving transformations enabled by auxiliary surface waves [50]. (a) Schematic of the structure, (b) Real part of the electric field $|\mathbf{Re}\{E_z\}|$ as obtained from full-wave simulations for a Taylor aperture antenna, (c) Theoretical and simulated radiation patterns.

reflections allowed the transformation to be accurately performed at a distance $d = 0.5\lambda$. The designed structure was simulated using three impedance layers for each HMS and the results are given in Figs. 12(b)–12(c). It can be observed that the wavefront acquires a planar profile with nearly constant amplitude, as desired. Moreover, the far-field radiation pattern matches very closely the theoretical, while around 95% of the incident power is transmitted to the output.

Lastly, surface waves have been investigated as a way to perform wave transformations that are characterized by different incident and output power profiles. Examples include beam splitting and perfect anomalous reflection with HMSs [51], as well as cloaking and beamforming with impenetrable impedance surfaces [52], [53]. Moreover, surface waves have been utilized in space-wave routing systems, where propagating power couples to surface waves on a metasurface section and gets relaunched from a different section of the whole metasurface system [54]. In the context of HMSs, surface waves are excited passively and modify the total input power so that the local power conservation is restored, and the metasurface can be designed as passive and lossless. Moreover, these auxiliary fields do not modify the far-field characteristics and do not result in reflected propagating power, since their spectrum is purely evanescent. While in relatively simple transformations (e.g., beam splitting, perfect anomalous reflection) the auxiliary fields can be analytically defined, more complicated applications require an optimization method.

In a recent work, beamforming was also demonstrated with a single Omega-bianisotropic transmissive HMS by utilizing auxiliary surface waves [50], as illustrated in Fig. 13(a). The auxiliary surface wave distribution was expanded in a set of basis functions with unknown complex weights A_n, similarly to the approach employed in the HMS pair design. However, in this case, the basis functions were modulated at a spatial frequency k_c so that their spectrum falls entirely within the evanescent part. By using superposition of the incident fields and the surface waves, the total input power was calculated as a function of the unknown weights A_n. Then, several equally spaced points along the HMS were selected to enforce local power conservation of the total fields at the two sides of the HMS. By minimizing the local power mismatch at the selected points using gradient descent optimization, a solution in terms of the weights A_n is found. Finally, knowing the incident, auxiliary and output fields, the HMS parameters are calculated through analytical expressions and implemented through three impedance sheets in full-wave simulations. As shown in Figs. 13(b)–13(c), a single HMS of length 6λ was used to transform the fields of a single current line source placed only $\lambda/3$ away from the HMS into the fields of a Taylor aperture with -20 dB sidelobe level. The remarkable agreement between the desired and simulated transmitted fields and the compactness of the design compared to cavity-exited HMSs or HMS pairs inspire further investigation of the above concept with physical structures.

E. RECONFIGURABLE HUYGENS' METASURFACES

Heretofore in this paper, passive HMSs have been discussed whose functionalities are inherently fixed to the geometrical parameters of their constituent meta-atoms. Although these passive HMSs offer extreme beam manipulation capabilities, many practical applications (e.g., high-rate communications, remote sensing, imaging, and radar) also require the ability to *dynamically* control various aspects of EM waves. In this regard, much of the recent effort has been devoted to the realization of reconfigurable metasurfaces. Nevertheless, the realization of a reconfigurable HMS for dynamic and independent control of both the *amplitude* and *phase* of an EM wave has been challenging due to the difficulties in locally tuning both electric and magnetic responses of individual meta-atoms and designing a biasing circuitry that would not degrade the microwave performance of the metasurface. As such, early research mainly focused on steering a reflected or transmitted beam by dynamically controlling only the phase along their surfaces which were in the form of reflect- and transmit-arrays, and impedance surfaces [55]–[59]. Although these early surfaces may not be of Huygens' type metasurfaces, we briefly review some of them which, in particular rely on active circuit elements for acquiring the necessary tunability. While there are other means to attain the tunability such as the utilization of phase transition materials (e.g., vanadium dioxide [60] and germanium-antimony-tellurium [61]), these methods are still not mainstream and are typically used in the Terahertz and optical regimes. For our purpose, we will focus our discussion to those that utilize variable microwave devices such as varactor diodes, PIN diodes, and micro-electromechanical (MEMS) switches. Following a review, we present our latest effort in the realization of a reconfigurable HMS that allows dynamic control of both the *amplitude* and *phase* of the reflection and transmission coefficients.

In the microwave regime, the integration of active lumped elements in the design of a unit cell has been extensively investigated to dynamically control the reflection or transmission phase from 0° to 360° at the highest possible reflection or transmission amplitude. Some of the early reconfigurable surfaces include various reflect-arrays that utilize varactor diodes [55]. In these surfaces, the capacitance of varactor diodes inside each unit cell is electronically altered by applying suitable bias voltages to dynamically modify the reflection phase profiles on their surfaces, thereby dynamically engineering the reflected wavefront. Instead of varactor diodes, PIN diodes and micro-electromechanical (MEMS) switches have also been frequently utilized to dynamically control the local reflection phases by discretely shorting or disconnecting some components inside the meta-atoms [62], [63]. On the other hand, those that operate in transmission mode have also been demonstrated which rely on a so-called Antenna-Filter-Antenna (AFA) architecture [56], [57]. The AFA architecture consists of arrays of receiving and transmitting patch antennas with reconfigurable unit cells in between that typically consist of MEMS switches, PIN or varactor diodes. The receiving antennas take an incoming EM wave and the unit cells add certain transmission phases to the wave which gets re-radiated by the transmitting antennas. Based on the AFA architecture, researchers have demonstrated dynamic tuning of the transmission phases for over 360° [56]. Instead of continuous variation, dynamic wavefront engineering based on discrete phase variation has also been demonstrated [64], [65].

The reconfigurable metasurfaces discussed thus far mainly focus on tuning the reflection or transmission phase profiles along their surfaces. However, provided that $\overline{\overline{Z}}_{\rm se}$, $\overline{\overline{Y}}_{\rm sm}$, and $\overline{\overline{K}}_{\rm em}$ can be arbitrarily and dynamically tuned, it is possible to realize a reconfigurable O-BHMS that can dynamically control both the amplitude and phase of the reflected and transmitted fields. However, such a realization is especially challenging because both electric and magnetic responses of individual meta-atoms need to be precisely tuned. Nevertheless, a few reconfigurable non-bianisotropic HMSs have been recently reported [66], [67]. In particular, the authors in [67] have employed the wire-loop topology to realize a Huygens' unit cell and integrated one varactor diode to the wire and two varactor diodes to the loop. By separately applying different bias voltages to these diodes, the authors demonstrated independent tuning of the electric and magnetic resonances and realized a reconfigurable meta-lens. Nevertheless, due to the aforementioned difficulty, the demonstrated functionality was also limited to dynamically controlling just the transmission phase profile, however, with improved transmission efficiency.

In order to completely and dynamically control the scattered EM fields (i.e., dynamic amplitude and phase control), we have recently proposed a reconfigurable O-BHMS by cascading four tunable impedance layers as shown in Fig. 14(a) [68]. Each layer consists of an array of dual-loop unit cell as shown in Fig. 14(b). For the unit cell, a varactor diode (MAVR-000120-14110P from MACOM) was integrated on the outermost loop to obtain the reconfigurability by applying

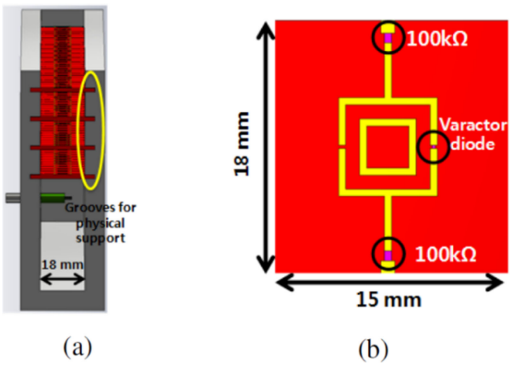

FIGURE 14. (a) The overview of the Huygens'-metasurface- assisted reconfigurable LWA and (b) the proposed tunable dual-loop unit cell. Reproduced figure from [69].

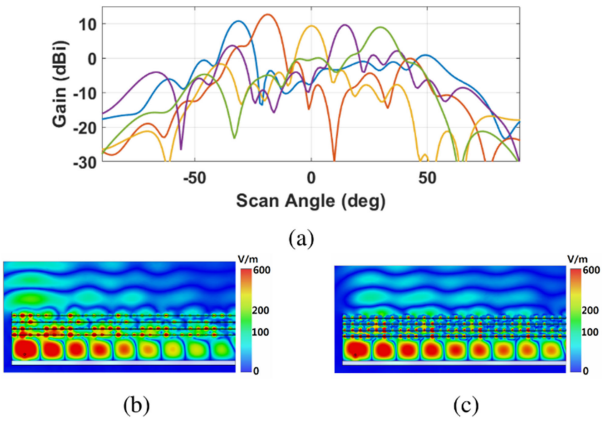

FIGURE 15. (a) The gain scan result with the tunable O-BHMS, and the electric field profiles of the reconfigurable LWA that radiates at broadside with (b) $\alpha = 0.035k_o$ and (c) $\alpha = 0.015k_o$.

DC bias voltage to it. Additionally, two 100 kΩ resistors were included at the two ends of the bias lines to decouple the radio-frequency waves and DC biasing circuitry. The proposed surface was then integrated inside a leaky-wave antenna (LWA) to form a compact antenna system similar to its passive version in [22]. It should be noted that the biasing lines can be accessed from outside by perforating the waveguide wall [69]. By applying suitable bias voltages to each unit cell, the local reflection and transmission coefficients of the surface can be independently and dynamically tuned. Since the proposed tunable O-BHMS allows independent control over its scattering parameters, an arbitrary guided mode can be supported and transformed to a certain desired radiation. In other words, the LWA allows independent and dynamic control of (i) the radiation angle (including broadside), (ii) leakage constant, and (iii) phase constant of a guided mode. As a demonstration, Fig. 15(a) shows the full-wave simulation results based on the proposed physical structure for a beam steering from −30° to +30° including broadside. In the simulation, the diodes from MACOM were modeled as lumped RLC boundaries whose resistance and capacitance values were obtained from Advanced Design System simulations. Furthermore, Figs. 15(b)

and 15(c) show two field profiles for broadside radiation with two different leakage constants from which it is clearly seen that the guided mode in Fig. 15(b) decays faster than that of the one shown in Fig. 15(c).

The discussion thus far has reviewed some of the reconfigurable metasurfaces that interact with an EM wave from an external source. However, a brief mention must also be given to *active* HMSs that utilize impressed Huygens' sources for generating electric and magnetic currents which are deduced from the equivalence principle [70]–[73]. For example, Selvanayagam *et al*. have demonstrated active cloaking by surrounding an object with impressed Huygens' sources that radiate a secondary scattered field which would destructively interfere with the primary scattered field caused by the incident field [70], [71]. Following this demonstration, a so-called Huygens' box was proposed which engineers the EM field within a region enclosed by impressed Huygens' sources [74]. In particular, Wong *et al*. have demonstrated the generation of propagating plane waves inside a metallic cavity by peripherally placing current strips in close proximity to the cavity walls. Recently, the idea of the Huygens' box was further developed to realize peripherally-excited phased arrays [74]–[76]. By synthesizing various propagating plane waves inside a Huygens' box and perforating its top plate to allow radiation, researchers have demonstrated steering of a pencil beam and generation of multiple beams with significantly reduced number of active components compared to traditional phased arrays albeit with a reduction of the scanning angular space [74]–[76].

V. OUTLOOK

Huygens' metasurfaces are an emerging class of engineered surfaces for the manipulation of incident electromagnetic wavefronts. In their basic form they comprise sub-wavelength unit cells that act as Huygens' sources or scatterers (secondary sources): The fictitious sources that are used to explain wave phenomena such as wave propagation, reflection and refraction in the Huygens' principle are now physically realized to manipulate electromagnetic waves at will, in a natural and versatile way. For example, such HMSs can be used to manipulate the phase, magnitude and polarization state of an impinging wave whether this is a plane wave, a beam or the fields from a nearby feeding source. In this way, sub-wavelength thin HMSs can be designed to refract an incident wave at an arbitrary angle with zero or tailored reflections. Likewise, perfect 'anomalous' reflection can be achieved in which the reflected angle can be arbitrary compared to the incident angle and with ideally 100% reflection efficiency [51], [77]. The microwave applications can be numerous and some of them were described in this paper including thin lenses for enhancing the gain of scanning antennas, or increasing their scan range. Other examples include quasi-optical beam splitting at arbitrary angles, chiral polarization control (e.g., CPSS or polarization rotators), arbitrary antenna beamforming and even low-cost electronic beam steering.

We have primarily reviewed passive HMSs but exciting opportunities exist for active ones or electronically reconfigurable ones. For example, thin active Huygens' metasurfaces can be used for cloaking [78], wavefront and beam synthesis in cavities for microwave sub-wavelength imaging and medical therapy, as well as exterior cloaking [79]. An emerging exciting concept is the use of apertures with only active-element excitations in their periphery for beam steering (through the equivalence principle) to drastically reduce the number of active elements form N^2 to N (albeit with a reduced scan range) [74]–[76]. Another emerging area is that of optically transparent metasurfaces for enhancing or manipulating wave propagation for fifth-generation (5G) signals in smart buildings or smart cars, e.g., using nanometer-scale silver films [80]. Finally, another area in which HMSs can play a significant role is that of time-varying metasurfaces for efficient frequency conversion [81], full-duplex communications (non-reciprocal) and/or novel beam steering at microwaves [82], [83].

REFERENCES

[1] R. E. Collin, *Field Theory of Guided Waves*, 2nd ed. Hoboken, NJ, USA: Wiley, 1990, ch. 12.

[2] V. G. Veselago, "The electrodynamics of substances with simultaneously negative values of ε and μ," *Sov. Phys. Usp.*, vol. 10, no. 4, pp. 509–514, Jan. 1968.

[3] R. A. Shelby, D. R. Smith, and S. Schultz, "Experimental verification of a negative index of refraction," *Science*, vol. 292, pp. 77–79, Apr. 2001.

[4] J. B. Pendry, A. J. Holden, D. J. Robbins, and W. J. Stewart, "Magnetism from conductors and enhanced nonlinear phenomena," *IEEE Trans. Microw. Theory Techn.*, vol. 47, no. 11, pp. 2075–2084, Nov. 1999.

[5] G. V. Eleftheriades and K. G. Balmain, *Negative-Refraction Metamaterials*. Hoboken, NJ, USA: IEEE/Wiley Press, 2005.

[6] C. Caloz and T. Itoh, *Electromagnetic Metamaterials: Transmission Line Theory and Microwave Applications*. Hoboken, NJ, USA: IEEE/Wiley Press, 2006.

[7] N. Yu *et al.*, "Light propagation with phase discontinuities: Generalized laws of reflection and refraction," *Science*, vol. 334, pp. 333–337, 2011.

[8] C. Huygens, *Traité De La Lumière*. Leiden, The Netherlands: Pierre vander Aa, 1690.

[9] C. Pfeiffer and A. Grbic, "Metamaterial Huygens' surfaces: Tailoring wave fronts with reflectionless sheets," *Phys. Rev. Lett.*, vol. 110, May 2013, Art. no. 197401.

[10] F. Monticone, N. M. Estakhri and A. Alú, "Full control of nanoscale optical transmission with a composite metascreen," *Phys. Rev. Lett.*, vol. 110, no. 20, May 2013, Art. no. 203903.

[11] M. Selvanayagam and G. V. Eleftheriades, "Discontinuous electromagnetic fields using orthogonal electric and magnetic currents for wavefront manipulation," *Opt. Exp.*, vol. 21, no. 12, pp. 14409–14429, Jun. 2013.

[12] E. F. Kuester, M. A. Mohamed, M. Piket-May, and C. L. Holloway, "Averaged transition conditions for electromagnetic fields at metafilm," *IEEE Trans. Antennas Propag.*, vol. 51, no. 10, pp. 2641–2651, Oct. 2003.

[13] K. Achouri, M. A. Salem, and C. Caloz, "General metasurface synthesis based on susceptibility tensors," *IEEE Trans. Antennas Propag.*, vol. 63, no. 7, pp. 2977–2991, Jul. 2015.

[14] A. Epstein and G. V. Eleftheriades, "Huygens' metasurfaces via the equivalence principle: Design and applications," *J. Opt. Soc. Amer. B*, vol. 33, no. 2, pp. A31–A50, Feb. 2016.

[15] A. Epstein and G. V. Eleftheriades, "Arbitrary power-conserving field transformations with passive lossless omega-type bianisotropic metasurfaces," *IEEE Trans. Antennas Propag.*, vol. 64, no. 9, pp. 3880–3895, Sep. 2016.

[16] J. P. S. Wong, A. Epstein, and G. V. Eleftheriades, "Reflectionless wide angle refracting metasurfaces," *IEEE Antennas Wireless Propag. Lett.*, vol. 15, pp. 1293–1296, 2016.

[17] T. Niemi, A. O. Karilainen, and S. A. Tretyakov, "Synthesis of polarization transformers," *IEEE Trans. Antennas Propag.*, vol. 61, no. 6, pp. 3102–3111, Jun. 2013.

[18] M. Kim and G. V. Eleftheriades, "Design and demonstration of impedance-matched dual-band chiral metasurfaces," *Sci. Rep.*, vol. 8, no. 1, 2018, Art. no. 3449.

[19] M. Kim and G. V. Eleftheriades, "Design and experimental demonstration of impedance-matched circular-polarization-selective surfaces with spin-selective phase modulations," *Phys. Rev. Appl.*, vol. 13, Jan. 2020, Art. no. 014009.

[20] M. Chen, E. Abdo-Sánchez, A. Epstein, and G. V. Eleftheriades, "Theory, design, and experimental verification of a reflectionless bianisotropic Huygens' metasurface for wide-angle refraction," *Phys. Rev. B, Condens. Matter*, vol. 97, Mar. 2018, Art. no. 125433.

[21] J. P. S. Wong, M. Selvanayagam, and G. V. Eleftheriades, "Polarization considerations for scalar Huygens metasurfaces and characterization for 2-D refraction," *IEEE Trans. Microw. Theory Techn.*, vol. 63, no. 3, pp. 913–924, Mar. 2015.

[22] E. Abdo-Sánchez, M. Chen, A. Epstein, and G. V. Eleftheriades, "A leaky-wave antenna with controlled radiation using a bianisotropic Huygens' metasurface," *IEEE Trans. Antennas Propag.*, vol. 67, no. 1, pp. 108–120, Jan. 2019.

[23] M. Chen, A. Epstein, and G. V. Eleftheriades, "Design and experimental verification of a passive Huygens' metasurface lens for gain enhancement of frequency-scanning slotted-waveguide antennas," *IEEE Trans. Antennas Propag.*, vol. 67, no. 7, pp. 4678–4692, Jul. 2019.

[24] G. Xu, S. V. Hum, and G. V. Eleftheriades, "Augmented Huygens' metasurfaces employing baffles for precise control of wave transformations," *IEEE Trans. Antennas Propag.*, vol. 67, no. 11, pp. 6935–6946, Nov. 2019.

[25] A. Epstein, J. P. Wong, and G. V. Eleftheriades, "Cavity-excited Huygens' metasurface antennas for near-unity aperture illumination efficiency from arbitrarily large apertures," *Nature Commun.*, vol. 7, Jan. 2016, Art. no. 10360.

[26] V. S. Asadchy, Y. Ra'di, J. Vehmas, and S. A. Tretyakov, "Functional metamirrors using bianisotropic elements," *Phys. Rev. Lett.*, vol. 114, Mar. 2015, Art. no. 095503.

[27] V. S. Asadchy, I. A. Faniayeu, Y. Ra'di, S. A. Khakhomov, I. V. Semchenko, and S. A. Tretyakov, "Broadband reflectionless metasheets: Frequency-selective transmission and perfect absorption," *Phys. Rev. X*, vol. 5, no. 3, Jul. 2015, Art. no. 031005.

[28] C. Pfeiffer, and A. Grbic, ""Millimeter-wave transmitarrays for wavefront and polarization control," *IEEE Trans. Microw. Theory Techn.*, vol. 61, no. 12, pp. 4407–4417, Dec. 2013.

[29] C. Pfeiffer and A. Grbic, "Bianisotropic metasurfaces for optimal polarization control: Analysis and synthesis," *Phys. Rev. Appl.*, vol. 2, Oct. 2014, Art. no. 044011.

[30] C. Pfeiffer, C. Zhang, V. Ray, L. J. Guo, and A. Grbic, "High performance bianisotropic metasurfaces: Asymmetric transmission of light," *Phys. Rev. Lett.*, vol. 113, no. 2, Jul. 2014, Art. no. 023902.

[31] K. Achouri, B. A. Khan, S. Gupta, G. Lavigne, M. A. Salem, and C. Caloz, "Synthesis of electromagnetic metasurfaces: Principles and illustrations," *EPJ Appl. Metamater.*, vol. 2, Oct. 2015, Art. no. 12.

[32] G. Lavigne, K. Achouri, V. S. Asadchy, S. A. Tretyakov, and C. Caloz, "Susceptibility derivation and experimental demonstration of refracting metasurfaces without spurious diffraction," *IEEE Trans. Antennas Propag.*, vol. 66, no. 3, pp. 1321–1330, Mar. 2018.

[33] V. S. Asadchy, M. Albooyeh, S. N. Tcvetkova, A. Díaz-Rubio, Y. Ra'di, and S. A. Tretyakov, "Perfect control of reflection and refraction using spatially dispersive metasurfaces," *Phys. Rev. B*, vol. 94, Aug. 2016, Art. no. 075142.

[34] M. Chen and G. V. Eleftheriades, "Omega-bianisotropic wire-loop Huygens' metasurface for reflectionless wide-angle refraction," *IEEE Trans. Antennas Propag.*, vol. 68, no. 3, pp. 1477–1490, Mar. 2020.

[35] A. H. Dorrah, M. Chen, and G. V. Eleftheriades, "Bianisotropic Huygens' metasurface for wideband impedance matching between two dielectric media," *IEEE Trans. Antennas Propag.*, vol. 66, no. 9, pp. 4729–4742, Sep. 2018.

[36] A. Epstein and G. V. Eleftheriades, "Passive lossless Huygens metasurfaces for conversion of arbitrary source field to directive radiation," *IEEE Trans. Antennas Propag.*, vol. 62, no. 11, pp. 5680–5695, Nov. 2014.

[37] G. A. Egorov and G. V. Eleftheriades, "Theory and simulation of metasurface lenses for extending the angular scan range of phased arrays," *IEEE Trans. Antennas Propag.*, vol. 68, no. 5, pp. 3705–3717, May 2020.

[38] Y. Zhao, M. A. Belkin, and A. Alù, "Twisted optical metamaterials for planarized ultrathin broadband circular polarizers," *Nature Commun.*, vol. 3, May 2012, Art. no. 870.

[39] A. N. Askarpour, Y. Zhao, and A. Alù, "Wave propagation in twisted metamaterials," *Phys. Rev. B*, vol. 90, Aug 2014, Art. no. 054305.

[40] M. Selvanayagam and G. V. Eleftheriades, "Polarization control using tensor Huygens' surfaces," *IEEE Trans. Antennas Propag.*, vol. 62, no. 12, pp. 6155–6168, Dec. 2014.

[41] M. Selvanayagam and G. V. Eleftheriades, "Design and measurement of tensor impedance transmitarrays for chiral polarization control," *IEEE Trans. Microw. Theory Techn.*, vol. 64, no. 2, pp. 414–428, Feb. 2016.

[42] H. Kazemi, M. Albooyeh, and F. Capolino, "Simultaneous perfect bending and polarization rotation of electromagnetic wavefront using chiral gradient metasurfaces," *Phys. Rev. Appl.*, vol. 13, Feb. 2020, Art. no. 024078.

[43] A. Khanikaev *et al.*, "Experimental demonstration of the microscopic origin of circular dichroism in two-dimensional metamaterials," *Nature Commun*, vol. 7, Jun. 2016, Art. no. 12045.

[44] Z. Li, D. Rosenmann, D. A. Czaplewski, X. Yang, and J. Gao, "Strong circular dichroism in chiral plasmonic metasurfaces optimized by micro-genetic algorithm," *Opt. Exp.*, vol. 27, no. 20, pp. 28313–28323, Sep. 2019.

[45] A. Epstein and G. V. Eleftheriades, "Arbitrary antenna arrays without feed networks based on cavity-excited omega-bianisotropic metasurfaces," *IEEE Trans. Antennas Propag.*, vol. 65, no. 4, pp. 1749–1756, Apr. 2017.

[46] S. A. H. Farahabadi, A. Bakhtafrouz, and A. Z. Nezhad, "Designing a reflectionless and bianisotropic metasurface antenna using dihedral corner reflector excitation," *J. Opt. Soc. Amer. B*, vol. 36, no. 6, pp. 1447–1456, Jun. 2019.

[47] B. O. Raeker and A. Grbic, "Compound metaoptics for amplitude and phase control of wave fronts," *Phys. Rev. Lett.*, vol. 122, Mar. 2019, Art. no. 113901.

[48] A. H. Dorrah and G. V. Eleftheriades, "Bianisotropic Huygens' metasurface pairs for nonlocal power-conserving wave transformations," *IEEE Antennas Wireless Propag. Lett.*, vol. 17, no. 10, pp. 1788–1792, Oct. 2018.

[49] V. G. Ataloglou, A. H. Dorrah, and G. V. Eleftheriades, "Design of compact Huygens' metasurface pairs with multiple reflections for arbitrary wave transformations," *IEEE Trans. Antennas Propag.*, vol. 68, no. 11, pp. 7382–7394, Nov. 2020.

[50] V. G. Ataloglou and G. V. Eleftheriades, "Surface-waves optimization for beamforming with a single omega-bianisotropic Huygens' metasurface," in *Proc. IEEE Int. Symp. Antennas Propag. USNC-URSI Radio Sci. Meet.*, Jul. 2020, Paper TH-A2.2A.7.

[51] A. Epstein and G. V. Eleftheriades, "Synthesis of passive lossless metasurfaces using auxiliary fields for reflectionless beam splitting and perfect reflection," *Phys. Rev. Lett.*, vol. 117, Dec. 2016, Art. no. 256103.

[52] D. H. Kwon and S. A. Tretyakov, "Arbitrary beam control using passive lossless metasurfaces enabled by orthogonally polarized custom surface waves," *Phys. Rev. B*, vol. 97, Jan. 2018, Art. no. 035439.

[53] D. H. Kwon, "Modulated reactance surfaces for leaky-wave radiation based on complete aperture field synthesis," *IEEE Trans. Antennas Propag.*, vol. 68, no. 7, pp. 5463–5477, Jul. 2020.

[54] K. Achouri and C. Caloz, "Space-wave routing via surface waves using a metasurface system," *Sci. Rep.*, vol. 8, May 2018, Art. no. 7549.

[55] S. V. Hum, M. Okoniewski, and R. J. Davies, "Realizing an electronically tunable reflectarray using varactor diode-tuned elements," *IEEE Microw. Wireless Compon. Lett.*, vol. 15, no. 6, pp. 422–424, Jun. 2005.

[56] J. Y. Lau and S. V. Hum, "A wideband reconfigurable transmitarray element," *IEEE Trans. Antennas Propag.*, vol. 60, no. 3, pp. 1303–1311, Mar. 2012.

[57] J. Y. Lau and S. V. Hum, "Reconfigurable transmitarray design approaches for beamforming applications," *IEEE Trans. Antennas Propag.*, vol. 60, no. 12, pp. 5679–5689, Dec. 2012.

[58] D. Sievenpiper *et al.*, "Electronic beam steering using a varactor-tuned impedance surface," in *Proc. Antennas Propag. Soc. Int. Symp.*, 2001, vol. 1, pp. 174–177.

[59] D. Sievenpiper and J. Schaffner, "Beam steering microwave reflector based on electrically tunable impedance surface," *Electron. Lett.*, vol. 38, no. 21, pp. 1237–1238, Oct. 2002.
[60] M. Kim, J. Jeong, J. K. S. Poon, and G. V. Eleftheriades, "Vanadium-dioxide-assisted digital optical metasurfaces for dynamic wavefront engineering," *J. Opt. Soc. Amer. B*, vol. 33, no. 5, pp. 980–988, May 2016.
[61] P. Hosseini, C. D. Wright, and H. Bhaskaran, "An optoelectronic frame-work enabled by low-dimensional phase-change films," *Nature*, vol. 511, no. 7508, pp. 206–211, Jul 2014.
[62] H. Rajagopalan, Y. Rahmat-Samii, and W. A. Imbriale, "RF MEMS actuated reconfigurable reflectarray patch-slot element," *IEEE Trans. Antennas Propag.*, vol. 56, no. 12, pp. 3689–3699, Dec. 2008.
[63] H. Kamoda, T. Iwasaki, J. Tsumochi, and T. Kuki, "60-GHz electrically reconfigurable reflectarray using P-I-N diode," in *IEEE MTT-S Int. Microw. Symp. Dig.*, Jun. 2009, pp. 1177–1180.
[64] A. Clemente, L. Dussopt, R. Sauleau, P. Potier, and P. Pouliguen, "1-bit reconfigurable unit cell based on pin diodes for transmit-array applications in X-band," *IEEE Trans. Antennas Propag.*, vol. 60, no. 5, pp. 2260–2269, May 2012.
[65] T. J. Cui, M. Q. Qi, X. Wan, J. Zhao, and Q. Cheng, "Coding metamaterials, digital metamaterials and programmable metamaterials," *Light, Sci. Appl.*, vol. 3, no. 10, Oct. 2014, Paper e218.
[66] K. Chen *et al.*, "A reconfigurable active Huygens' metalens," *Adv. Mater.*, vol. 29, no. 17, 2017, Art. no. 1606422.
[67] M. Y. Xu and S. V. Hum, "Realization of low-complexity reconfigurable Huygens' metasurfaces," in *Proc. 13th Eur. Conf. Antennas Propag. (EuCAP)*, 2019, pp. 1–4.
[68] M. Kim and G. V. Eleftheriades, "Reconfigurable leaky-wave antennas with independent control of the leakage constant and radiation angle," in *Proc. 14th Eur. Conf. Antennas Propag.*, 2020, pp. 1–5.
[69] M. Kim and G. V. Eleftheriades, "Huygens'-metasurface-assisted reconfigurable leaky-wave antennas with dynamically-controlled radiation patterns," in *Proc. 14th Int. Congr. Artif. Materials Novel Wave Phenomena (Metamaterials)*, New York, NY, USA, 2020, pp. 1–3.
[70] M. Selvanayagam and G. V. Eleftheriades, "An active electromagnetic cloak using the equivalence principle," *IEEE Antennas Wireless Propag. Lett.*, vol. 11, pp. 1226–1229, 2012.
[71] M. Selvanayagam and G. V. Eleftheriades, "Experimental demonstration of active electromagnetic cloaking," *Phys. Rev. X*, vol. 3, Nov. 2013, Art. no. 041011.
[72] A. M. H. Wong and G. V. Eleftheriades, "Experimental demonstration of the Huygens' box: Arbitrary waveform generation in a metallic cavity," in *Proc. IEEE Int. Symp. Antennas Propag. USNC/URSI Nat. Radio Sci. Meet.*, Jul. 2018, pp. 1893–1894.
[73] P. Ang and G. V. Eleftheriades, "Active cloaking of a non-uniform scatterer," *Sci. Rep.*, vol. 10, no. 1, Feb. 2020, Art. no. 2021.
[74] K. A. Oyesina and A. M. H. Wong, "The Huygens' box antenna: Metasurface-based directive antenna beam-steering with dramatically reduced elements," in *Proc. IEEE Int. Symp. Antennas Propag. USNC-URSI Radio Sci. Meet.*, Jul. 2019, pp. 443–444.
[75] A. Dorrah and G. V. Eleftheriades, "Peripherally excited phased arrays: Beam steering with reduced number of antenna elements," in *Proc. IEEE Can. Conf. Elect. Comput. Eng.*, May 5-8, 2019, pp. 1–4.
[76] A. H. Dorrah and G. V. Eleftheriades, "Peripherally excited phased array architecture for beam steering with reduced number of active elements," *IEEE Trans. Antennas Propag.*, vol. 68, no. 3, pp. 1249–1260, Mar. 2020.
[77] A. M. H. Wong and G. V. Eleftheriades, "Perfect anomalous reflection with a bipartite Huygens' metasurface," *Phys. Rev. X*, vol. 8, Feb. 2018, Art. no. 011036.
[78] P. Ang and G. V. Eleftheriades, "Experimental active cloaking of a metallic polygonal cylinder," *Proc. IEEE MTT-S Int. Microw. Symp.*, Jun. 2-7, 2019, pp. 39–42.
[79] A. M. H. Wong and G. V. Eleftheriades, "Active Huygens' box: Arbitrary electromagnetic wave generation with an electronically controlled metasurface," *IEEE Trans. Antennas Propagat.*, early access, Aug. 24, 2020, doi: 10.1109/TAP.2020.3017438.
[80] M. Safari, Y. He, M. Kim, N. P. Kherani, and G. V. Eleftheriades, "Optically and RF transparent Meta-glass," *De Gruyter Nanophoton.*, vol. 9, no. 12, pp. 3889–3898, Jun. 2020, doi: 10.1515/nanoph-2020-0056.
[81] Z. Wu and A. Grbic, "Serrodyne frequency translation using time-modulated metasurfaces," *IEEE Trans. Antennas Propag.*, vol. 68, no. 3, pp. 1599–1606, Mar. 2020.
[82] J. Zang, D. Correas-Serrano, J. T. S. Do, X. Liu, A. Alvarez-Melcon, and J. Gomez-Diaz, "Nonreciprocal wavefront engineering with time-modulated gradient metasurfaces," *Phys. Rev. Appl.*, vol. 11, no. 5, May 2019, Art. no. 054054.
[83] S. Taravati and G. V. Eleftheriades, "Full-duplex nonreciprocal beam steering by time modulated phase-gradient metasurfaces," *Phys. Rev. Appl.*, vol. 14, Jul. 2020, Art. no. 014027.